ARTICLES
https://doi.org/10.1038/s41592-020-0731-1

nature methods

Measurement of atom resolvability in cryo-EM maps with *Q*-scores

Grigore Pintilie[1*], Kaiming Zhang[1], Zhaoming Su[1], Shanshan Li[1], Michael F. Schmid[2] and Wah Chiu[1,2*]

Cryogenic electron microscopy (cryo-EM) maps are now at the point where resolvability of individual atoms can be achieved. However, resolvability is not necessarily uniform throughout the map. We introduce a quantitative parameter to characterize the resolvability of individual atoms in cryo-EM maps, the map *Q*-score. *Q*-scores can be calculated for atoms in proteins, nucleic acids, water, ligands and other solvent atoms, using models fitted to or derived from cryo-EM maps. *Q*-scores can also be averaged to represent larger features such as entire residues and nucleotides. Averaged over entire models, *Q*-scores correlate very well with the estimated resolution of cryo-EM maps for both protein and RNA. Assuming the models they are calculated from are well fitted to the map, *Q*-scores can be used as a measure of resolvability in cryo-EM maps at various scales, from entire macromolecules down to individual atoms. *Q*-score analysis of multiple cryo-EM maps of the same proteins derived from different laboratories confirms the reproducibility of structural features from side chains down to water and ion atoms.

Cryogenic electron microscopy (cryo-EM) single-particle methods strive to create accurate, high-resolution three-dimensional maps of macromolecules. Depending on many factors, including imaging apparatus, detector, reconstruction method, structure flexibility, sample heterogeneity and differential radiation damage, resulting maps have varying degrees of resolvability. Accurate quantification of resolvability in cryo-EM maps has been a challenge in the field[1]. This task is very important as it can affect the interpretation of such maps.

For every cryo-EM map, a resolution is estimated from a Fourier shell correlation (FSC) plot between two independent reconstructions, each reconstruction stemming from a separate half of the data set[2]. It is well recognized that cryo-EM maps usually do not have isotropic resolution throughout, and thus local resolution is typically estimated, for example with ResMap[3], Bsoft[4] or MonoRes[5]. However, such local resolutions do not easily translate to particular features of interest such as side chains or individual atoms.

Atomic models can be either fitted or built directly into cryo-EM maps[6,7]. Map-model scores are then calculated to assess how well the model fits the map[8]. Real-space refinement[9] or flexible fitting[10,11] can be applied, making sure to not overfit to noise[12,13]. The latter is accomplished through stereochemical restraints, for example bond lengths, angles, dihedrals, preferred rotamers and van der Waals distances, and additional secondary-structure constraints, for example in the form of hydrogen bonds[9,11,14,15].

Once an atomic model has been fitted to or derived from a cryo-EM map, it can then be used to assess the map itself. This can be done in several ways, including a map-model FSC curve, which requires that the model first be converted to a cryo-EM-like map at the same resolution as the original map. Such an FSC plot reflects the entire map volume. Proper masking may be used to assess smaller features such as individual protein chains[12]; however, it is impractical to assess even smaller features such as side chains or individual atoms using this approach.

Other methods that assess smaller features in a cryo-EM map using a fitted model include EMRinger[16] and *Z*-scores[17]. EMRinger considers map values near carbon-β atoms, while *Z*-scores can be applied to secondary-structure elements (such as α-helices and β-sheets) or side chains. These scores were shown to correlate with map resolution when averaged over entire maps and models. Moreover, they can also identify features in the model (for example, secondary-structure elements or side chains) that are not well resolved or not fitted properly to the map.

Cryo-EM maps have reached resolutions nearer to atomic dimensions, for example, apoferritin at 1.54 Å (Electron Microscopy Data Bank (EMDB) 9865), 1.62 Å (EMDB 0144)[18], 1.65 Å (EMDB 0599) and 1.75 Å (EMDB 20026). At such resolutions, we may start to assess the resolvability of individual atoms. In crystallography, B-factors or atomic displacement parameters (ADPs) reflect the uncertainty in the position of any atom, and are refined from diffraction data[19–21]. ADPs can also be calculated in cryo-EM maps[22]. However, since ADPs are typically refined with restraints, they are not dependent only on the map values around the atom. Other ways to measure positional uncertainties include multi-model refinement[23] and molecular dynamics;[12,24] these also assume various restraints on atoms and hence do not reflect map values alone.

In this paper, we introduce *Q*-scores, which are calculated directly from map values around an atom's position. A similar score is the electron density score, EDIA[25], which has been applied to high-resolution X-ray maps. The EDIA method considers map values within each atom's radius, which is parameterized for different elements and resolutions. In contrast, *Q*-scores are calculated independently of element type or map resolution. We apply *Q*-scores to measure resolvability of individual atoms, including solvent atoms, and also of groups of atoms such as side chains in proteins and bases in nucleic acids.

Results

Atomic map profiles. Atomic map profiles show average map values at increasing radial distances from an atom's position. Only points that are closer to the atom in question than to any other atom in the model are considered. Figure 1a shows example atomic

[1]Department of Bioengineering, James H. Clark Center, Stanford University, Stanford, CA, USA. [2]Division of CryoEM and Bioimaging, SSRL, SLAC National Accelerator Laboratory, Stanford University, Menlo Park, CA, USA. *e-mail: gregp@slac.stanford.edu; wahc@stanford.edu

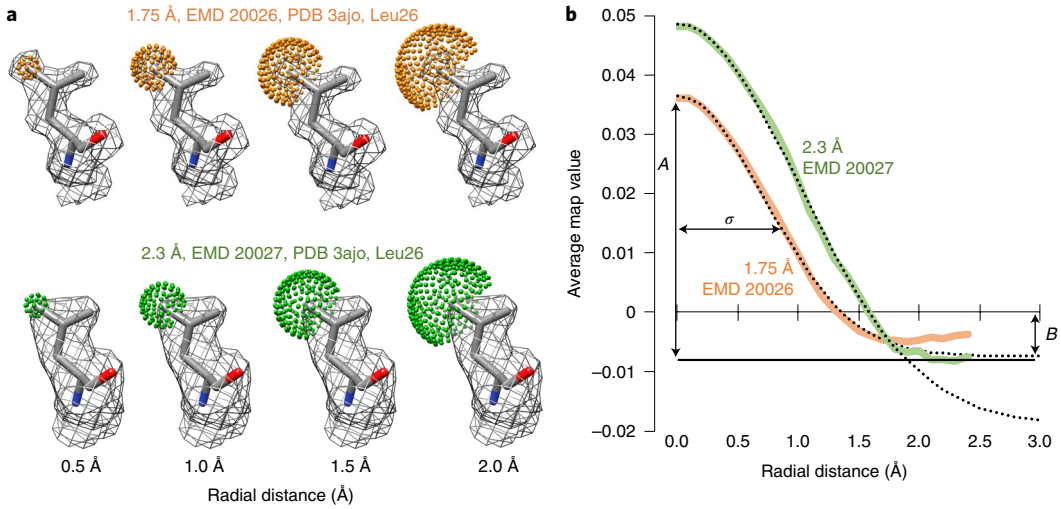

Fig. 1 | Atomic map profiles in cryo-EM two maps of apoferritin. a, The residue Leu26 in the fitted model (PDB 3ajo) is shown, along with contour surface of the cryo-EM map around this residue. Spherical shells of points centered on the CD2 atom are shown at increasing radial distances. Only points that are closer to the CD2 atom than to any other atom in the model are used to calculate an average map value at each radial distance. **b**, Plots of average map value versus radial distance; these are the atomic map profiles. The dotted lines represent Gaussian functions that are fitted to each profile.

profiles in two new maps of apoferritin with resolutions of 1.75 and 2.32 Å, deposited as EMDB 20026 and EMDB 20027.

When calculating the profile for an atom, map values at N points are used to calculate the average at a particular distance, r. The N points are distributed evenly across the part of the sphere (centered at the atom, with radius r) that is closer to the atom and not any other atom in the model. At $r=0$ or the atom center, the map value is duplicated N times, so that N is the same at each radial distance. In all calculations used here, we use $N=8$. Larger values of N typically create smoother profiles; however, they have only minor effects on Q-scores described below.

The model in Fig. 1 is the X-ray model of apoferritin (Protein Data Bank (PDB) ID 3ajo), which was first rigidly fitted to the cryo-EM map, and then further refined into each cryo-EM map using Phenix real-space refinement[9]. In the examples, atomic profiles have Gaussian-like contours. We consider a Gaussian equation of the form:

$$y = Ae^{-\frac{1}{2}\left(\frac{x-\mu}{\sigma}\right)^2} + B \tag{1}$$

Gaussian functions of the form in equation (1), where x is the radial distance and y the average map value, fit well to the atomic profiles shown in Fig. 1 up to a distance of 2 Å, with a mean error of 2.4%. For higher resolution data, for example from X-ray crystallography, multiple Gaussians are used to closely represent atomic form factors[25]; however, we do not consider that here. Past 2 Å from the atom, map profiles observed in these and other similar resolution cryo-EM maps become noisy and start to increase. This is likely due to effects from other nearby atoms and/or solvents.

When the model is well fitted to the map, the width of the Gaussian function (equation (1)) fitted to the profile, σ, may be considered to be proportional to factors such as the resolution of the map and the overall mobility of the atom. Regardless of the cause, in this paper we assume that the profile seen in the map indicates to what degree the atom is resolved: narrower profiles indicate the atom is better resolved, while wider profiles indicate the atom is less well resolved.

***Q*-score.** The Q-score measures how similar map values around an atom are to a Gaussian-like function we would see if the atom is well resolved. Thus, to calculate it, the map values around the atom are compared to values from a 'reference Gaussian' as given by equation (1), with the following parameters:

$$\mu = 0 \tag{2}$$

$$A = \text{avg}_M + 10\sigma_M \tag{3}$$

$$B = \text{avg}_M - 1\sigma_M \tag{4}$$

$$\sigma = 0.6\text{Å} \tag{5}$$

In the above, the mean, μ, is set to 0, as the reference Gaussian is centered at the atom's position. The parameters A and B are obtained using the mean/average across all values in the entire map, avg_M, and the standard deviation of all values around this mean, σ_M. The width of the reference Gaussian is set as $\sigma=0.6$. These parameters were chosen to make the reference Gaussian roughly match the atomic profile of a well-resolved atom in the 1.54 Å cryo-EM map as shown in Fig. 2b.

The Q-score is calculated as a correlation between two vectors: $\mathbf{u}$, which contains map values at points around the atom, and $\mathbf{v}$, which contains values obtained from the reference Gaussian. Points around the atom are taken from spheres with increasing radii, as shown for the atomic profiles in Fig. 1. The map value for each point is calculated by trilinear interpolation using map values at the nearest eight grid points. The corresponding reference Gaussian value for each point is calculated using equation (1), with x being the radius of the sphere from which the point is taken. The vectors $\mathbf{u}$ and $\mathbf{v}$ contain $N\times M$ values, where N is the number of points at each radial distance and M is the number of radial distances sampled between 0 and 2 Å. Here $N=8$, as described above for atomic profiles, and $M=21$, with distances sampled at 0.1-Å intervals. The following normalized about-the-mean cross-correlation formula is used to compare the two vectors:

$$\mathbf{Q} = \frac{\langle \mathbf{u} - \mathbf{u}_{\text{mean}} \rangle \langle \mathbf{v} - \mathbf{v}_{\text{mean}} \rangle}{|\mathbf{u} - \mathbf{u}_{\text{mean}}||\mathbf{v} - \mathbf{v}_{\text{mean}}|} \tag{6}$$

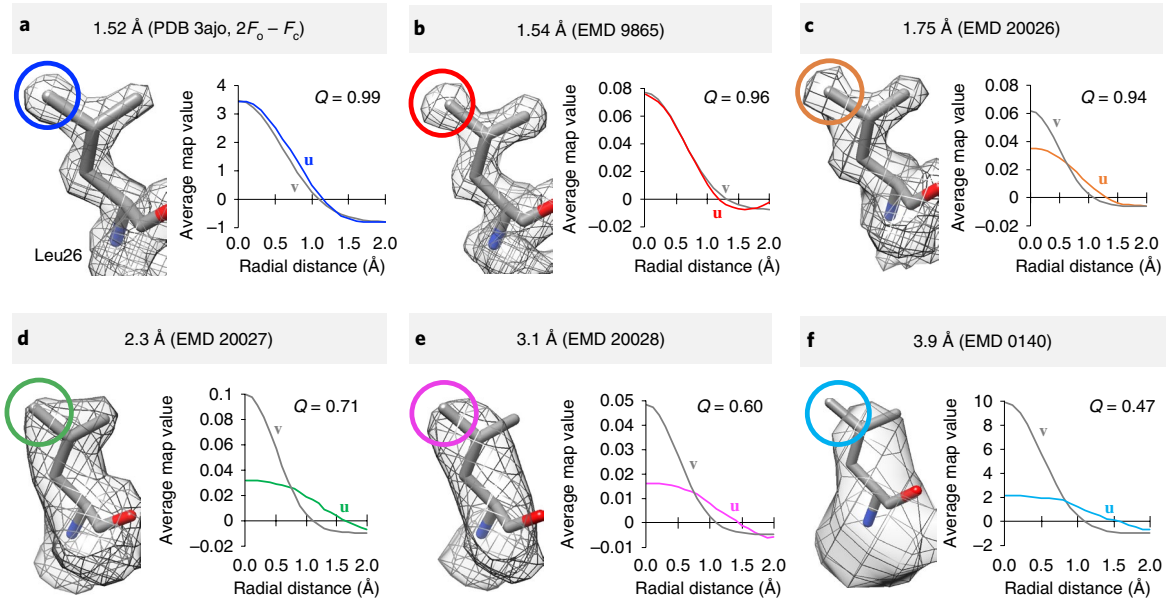

Fig. 2 | Calculation of *Q*-scores for an atom in six maps at different resolutions, including an X-ray map (PDB 3ajo). a–f, The atom is CD2 from Leu26 in the X-ray model PDB 3ajo fitted to each map. The atomic profile in each map is marked with the letter *u*, while the reference Gaussian is marked with ***v***. In **a** and **b**, which show maps at resolutions close to 1.5 Å, the atomic profiles are very similar to the reference Gaussians, and hence the *Q*-scores are high. In **c–f**, as the resolution of the map decreases, atomic profiles become wider and more flat compared to the reference Gaussian, and *Q*-score decreases accordingly.

Several atomic profiles and reference Gaussians are illustrated in Fig. 2. At resolutions close to 1.5 Å, the atomic profiles are very similar to the reference Gaussian, and hence *Q*-scores are close to their maximum value of 1. At lower resolutions, the atomic profiles of the same atom are wider than the reference Gaussian, hence *Q*-scores are lower. *Q*-scores would also be low for atomic profiles that are mostly noise (for example, random values or a sharp peak). In some cases when the atom is not well-placed in the map, the *Q*-score can be negative if the atomic profile has a shape that increases away from the atom's position.

Q-scores are low when the entire model is placed incorrectly in the map; for example, during a global search. They can increase if the model-map fit is improved by local refinement (Supplementary Fig. 1). *Q*-scores begin to decrease as resolutions of the map increase beyond 1.30 Å, as atomic profiles begin to be much narrower than the reference Gaussian (Supplementary Fig. 2). This effect may be useful in cryo-EM maps to give very sharp peaks, which are more likely to be noise, lower *Q*-scores.

Calculating *Q*-scores is similar to calculating a cross-correlation between the model and a cryo-EM map, using a simulated map of the model blurred using a Gaussian function with the parameters in equations (2)–(5). The main difference is that with *Q*-scores, the cross-correlation is performed atom-by-atom separating out parts of the map that are closest to each atom. The cross-correlation about the mean is used so that the *Q*-scores decrease as resolution also decreases. When not subtracting the mean, this effect would not be ensured, as shown previously[17] and also in Supplementary Fig. 3.

We tested the effect of several factors on *Q*-scores. First, using the cross-correlation about the mean makes the *Q*-scores insensitive to the height and vertical offset of the reference Gaussian (Supplementary Fig. 3). This means that as long as map values are decreasing around an atom, regardless of their relative magnitude in the map, the *Q*-score for the atom could still be high. Second, small changes in grid step and placement do not affect the *Q*-score; however, if the grid step is too large relative to the resolution of the map, resolvability and also *Q*-scores can start to decrease (Supplementary Fig. 4). Finally, sharpening can increase the visible detail in the map along with *Q*-scores, but *Q*-scores start to decrease if excessive sharpening is applied (Supplementary Fig. 5).

Q-scores of atoms in proteins. Figure 3 shows *Q*-scores for atoms taken from maps of apoferritin at various resolutions. One of the maps is an X-ray map at 1.52 Å resolution ($2F_o - F_c$, PDB 3ajo) as a reference; another is a recent high-resolution map at 1.54 Å (EMDB 9599). The other three are new maps we reconstructed to 1.75 Å (EMDB 20026), 2.3 Å (EMDB 20027) and 3.1 Å (EMDB 20028) with different numbers of particle images from the same data set. For the cryo-EM maps, the X-ray model PDB 3ajo was fitted to the map and refined using Phenix real-space refinement[9].

In Fig. 3, *Q*-scores for each atom correlate well with visual resolvability at the contour level used in each case; that is, the more resolvable an atom, the higher the *Q*-score. However, in some cases, the *Q*-score for an atom can be relatively high even if there is no map contour around it; this is due to the effect mentioned previously that even if the map values around an atom are low, the *Q*-score can still be high if they are decreasing away from the atom.

Resolvability and *Q*-scores can decrease for some residues faster than others as a function of resolution. For example, in Fig. 3, the *Q*-score for ASP126 drops more than for ASN25 from 1.52 to 3.9 Å. This effect may be due to several reasons. First, some residue types may be more susceptible to radiation damage (as previously shown using EMRinger[16]). Also, certain residue types may be more conformationally dynamic, or occur in environments that are more dynamic (for example, solvent accessible), and hence may not resolve as well with fewer number of particles. Finally, the interaction of the electron beam with negatively charged side chains may have a weakening effect on map values around them at lower resolutions[22].

Q-scores for atoms in nucleic acids. *Q*-scores can also be calculated for atoms in nucleic acids. In Fig. 4, we used several maps and models containing RNA from the EMDB at resolutions ranging from 2.5 to 4.0 Å. *Q*-scores were averaged over atoms in bases (labeled Q_{base}), phosphate-sugar backbones (labeled Q_{bb}) and entire nucleotides. As with proteins, *Q*-scores decrease with resolvability and estimated

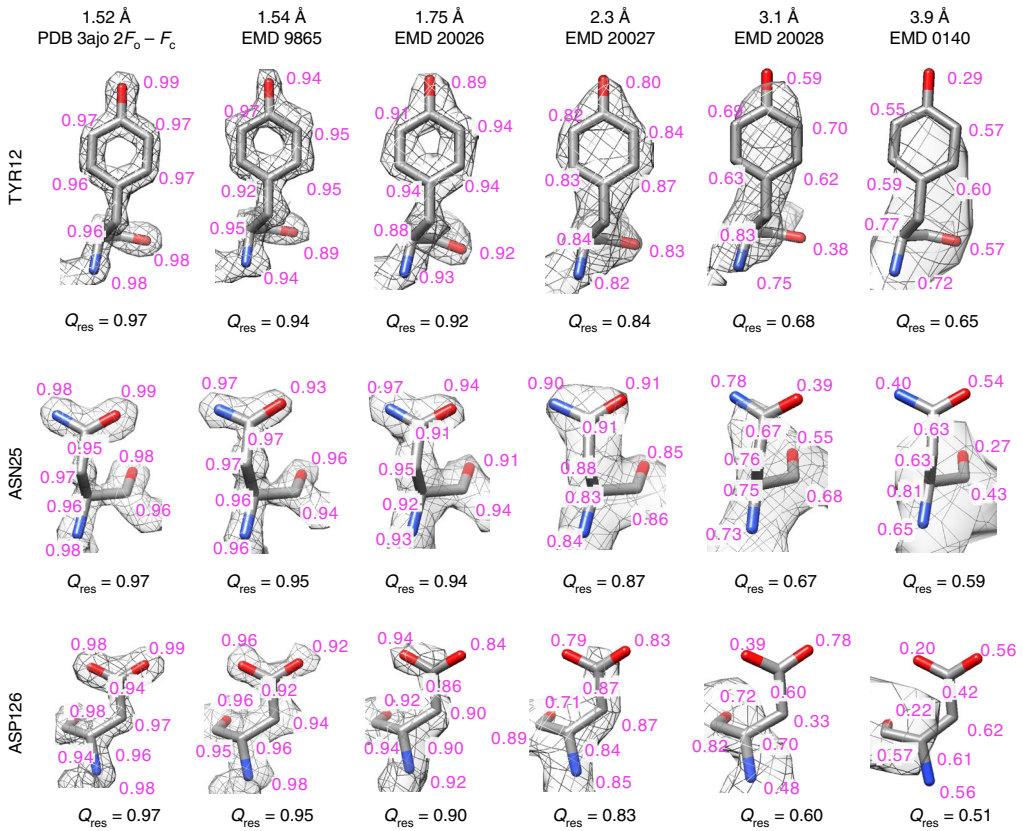

Fig. 3 | *Q*-scores for three residues taken from apoferritin maps at various resolutions. Atom *Q*-scores are shown close to each atom, and the average *Q*-score is shown under each residue.

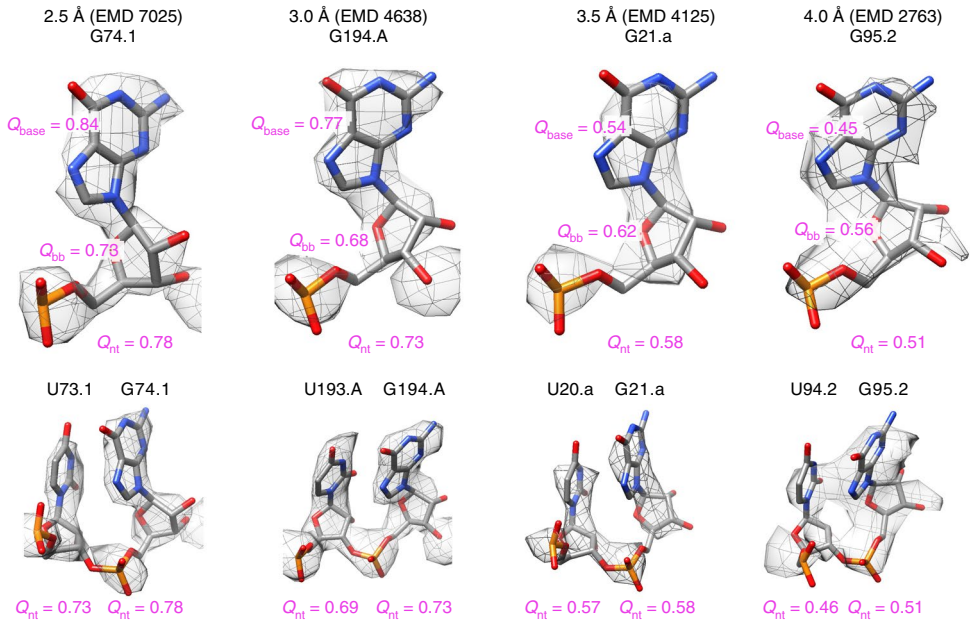

Fig. 4 | *Q*-scores averaged over nucleotides (Q_{nt}) in cryo-EM maps and models of ribosomes from the EMDB at four different resolutions. *Q*-scores are also averaged for base (Q_{base}) and phosphate-sugar backbone (Q_{bb}) atoms.

map resolution. Figure 4 also illustrates a general trend that at ~4 Å and lower resolutions, stacked bases from adjacent nucleotides are typically not separable in cryo-EM maps, whereas at higher than 4 Å resolutions, they usually do become separate at some contour levels.

It is also interesting to note that for the examples in Fig. 4, at higher resolutions (~2.5 Å), the difference in *Q*-score or resolvability of individual bases is higher than that of the backbone (0.84 for base versus 0.73 for backbone). Going toward lower resolutions in

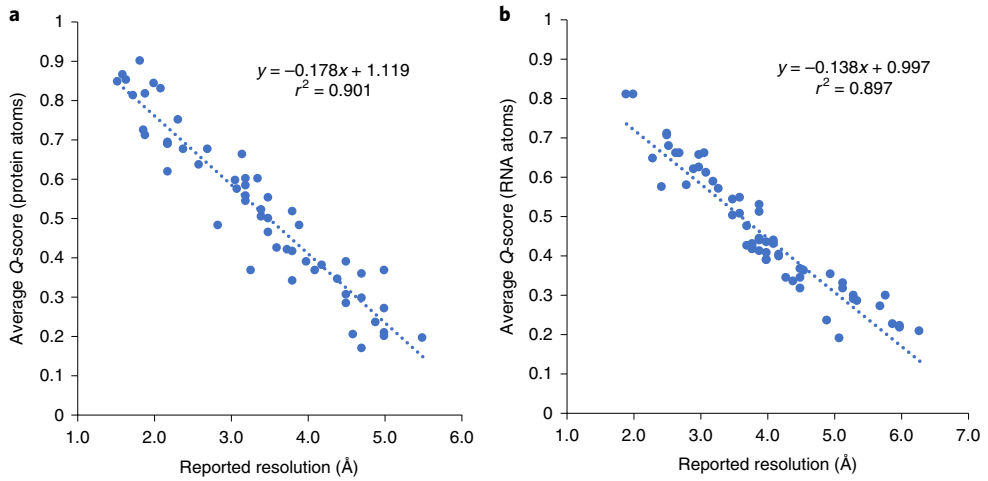

Fig. 5 | Average *Q*-scores versus reported resolution for maps and models obtained from the EMDB. a, *Q*-scores averaged over only protein atoms in maps and models listed in Supplementary Table 1. **b**, *Q*-scores averaged over only nucleic acid atoms in maps and models listed in Supplementary Table 2. Linear functions fitted to the points are drawn with a dotted line in both plots; equations and r^2 value are inset.

this example, bases become less resolvable (0.45 for bases versus 0.56 for backbone). This may be counter-intuitive as bases can have higher values in the map (that is, they appear first at a high contour level). However, these contours may have overall less detail as adjacent stacked bases are not fully separable at any contour level.

***Q*-score versus resolution.** *Q*-scores can also be averaged across an entire model to represent an average resolvability measure for the entire map. Such average *Q*-scores were plotted as a function of reported resolution for a number of maps and models obtained from the EMDB. Figure 5 shows these plots for two sets of maps and models, for one set using only atoms in proteins, and for the other set using only atoms in nucleic acids. The full sets are listed in Supplementary Tables 1 and 2. In both cases, the average *Q*-score correlates very strongly to reported resolution. This strong correlation indicates that *Q*-scores closely capture the resolvability of atomic features in cryo-EM maps, much as the estimated resolution of a map does. However, *Q*-scores are further useful in quantifying resolvability of local features within each map down to individual atoms.

The linear plots in Fig. 5 suggest that average *Q*-scores drop toward 0 at ~6–7 Å, however, an analysis using simulated maps indicates that they taper off and decrease slowly toward 0 at lower resolutions (Supplementary Fig. 6). Negative *Q*-scores would only be expected if atoms are not placed on peaks, such that map values increase away from their position. Nevertheless, due to the change in rate of decrease, we expect that *Q*-scores are most useful at resolutions better than 5–6 Å (refs. [26,27]).

***Q*-scores versus B-factors and ADPs.** B-factors and ADPs are used in X-ray crystallography to convey the positional uncertainty of atoms[19–21]. They are also dependent to some degree on resolution[28] (Supplementary Fig. 7). When refining B-factors and ADPs, various restraints, parameters and initial values can be used, hence the results in each map may vary. Comparisons of B-factors/ADPs to *Q*-scores show that they correlate only weakly (Supplementary Figs. 8 and 9). Hence, they likely convey somewhat different information.

***Q*-scores of solvent atoms.** The X-ray apoferritin structure (PDB 3ajo) contains one protein chain, 229 oxygen (O) atoms (from water) and 12 Mg atoms. A closeup on the structure is shown in Fig. 6, where it is also fitted to five cryo-EM maps at different resolutions. It is reassuring to see that some of the solvent atoms in the X-ray structure can also be observed in the cryo-EM maps (for example, Mg183, O280, O236). However, some of the atoms (for example, Mg184), are not seen equally well in all maps; for example, in the 1.54 and 1.65 Å maps, Mg184 has a low *Q*-score (0.12 and 0.03, respectively). Such differences may be due to different affinities at some sites and/or different biochemical conditions across the different data sets.

Distributions of *Q*-scores for solvent atoms in the X-ray map (PDB 3ajo) are shown in Supplemetary Fig. 10a. Most solvent atoms have very high *Q*-scores of 0.9 and higher. Visual inspection confirmed that all these solvent atoms can be seen in the X-ray map ($2F_o - F_c$), for example as shown in Fig. 6a. Supplementary Fig. 10b shows *Q*-score distribution plots for the same model rigidly fitted to the cryo-EM maps of apoferritin at 1.54 and 1.75 Å resolution. For these rigidly fitted models, *Q*-scores of the solvent atoms are considerably lower than in the X-ray map. For example, in the 1.75 Å cryo-EM map, only 44 of the 229 O atoms from water have *Q*-scores of 0.8 and higher. In the 1.54 Å map, 68 have *Q*-scores of 0.8 and higher. Thus, some of the solvent atoms in the X-ray structure may not be resolvable in these cryo-EM maps or may be in different positions.

To explore whether solvent atoms may have different positions in the cryo-EM maps, *Q*-scores of the solvent atoms were also calculated in the X-ray structure after real-space refinement with Phenix[9]. The distributions in the *Q*-scores for solvent atoms after this procedure are plotted in Supplementary Fig. 10c for the two cryo-EM maps. *Q*-scores are now higher; 142 water atoms in the 1.54 Å map and 145 atoms in the 1.75 Å map have *Q*-scores of 0.8 and higher, compared to 225 water atoms in the X-ray map with *Q*-scores of 0.8 and higher.

We further consider water atoms with *Q*-scores of 0.8 and higher after refinement, which can be considered to be well resolved in the cryo-EM maps. In the 1.54 Å map, the 142 water atoms with *Q*-scores 0.8 and higher moved between 0.1 and 2.2 Å, on average 0.54 Å. In the 1.75 Å map, the 145 water atoms with *Q*-scores of 0.8 and higher moved between 0.1 and 1.6 Å, on average 0.67 Å. Radial distance plots in Supplementary Fig. 11 show sharp peaks at ~2.8 Å for water–water and water–protein distances in X-ray maps, but more diffuse peaks around the same distance in cryo-EM maps.

Although it is difficult to assess the exact cause of these relatively small distance variations between X-ray and cryo-EM structures, it is reasonable to conclude that many of the waters in the X-ray structure are also resolved and near the same positions in cryo-EM maps.

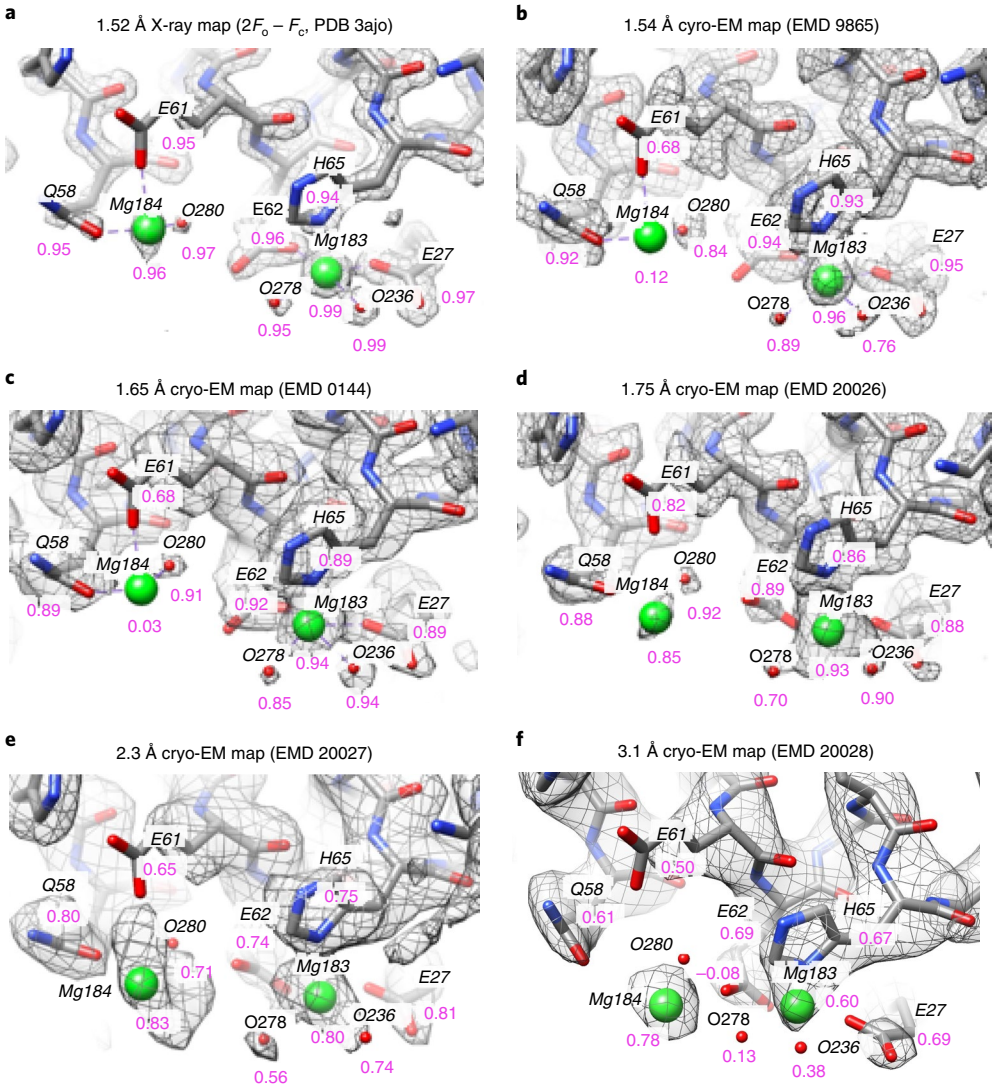

Fig. 6 | A close up in apoferritin maps showing solvent atoms (Mg and O from water), along with calculated *Q*-scores in purple under each atom and nearby residue. a, X-ray structure and map at 1.52 Å resolution; all solvent atoms are visible at the contour level shown and have high *Q*-scores. **b**–**d**, Same structure rigidly fitted to cryo-EM maps at resolutions of 1.54 Å, 1.65 Å and 1.75 Å; in these maps, some of the same solvent atoms are also clearly visible and have high *Q*-scores (for example, Mg183, O278, O280 and O236); other solvent atoms are not as visible and have low *Q*-scores (for example, Mg184). **e**,**f**, Maps at lower resolutions of 2.3 Å and 3.1 Å; Mg atoms are still visible, although the map contours around them are not as sharp and symmetrical and hence their *Q*-scores are lower. In **e**, one O atom is still visible (O278), although it has a lower *Q*-score. In **f**, the O atoms are not visible and have very low *Q*-scores.

Water networks have been shown to be important in ligand binding affinities and to vary due to structural differences even in X-ray structures[29]. Further studies with more cryo-EM maps at similar resolutions may further elucidate and characterize such variations.

In the above analysis, solvent atom positions were based on those originally observed in the X-ray structure. If one studies a de novo map, the identification of solvent atoms would require a protocol used in modeling software[30]. In addition to such a protocol, *Q*-scores may be useful as an additional parameter to assist in the finding of such solvent atoms.

***Q*-scores of solvent atoms at different resolutions.** Finally, we looked at the resolvability and *Q*-scores of solvent atoms in cryo-EM maps of apoferritin at different resolutions, as shown in Fig. 6. The locations of the solvent atoms are again taken from the X-ray structure (PDB 3ajo). Mg183 appears resolved at 1.75 and 2.3 Å, with separable contours in both maps and high *Q*-scores (0.93 and 0.80). In the 3.1 Å map, the contour is no longer separable from that of the nearby His65 residue, and the *Q*-score is also considerably lower (0.60). Some water atoms are also resolved in the 1.75 and 2.3 Å maps and contours around them can be seen, but at 3.1 Å they can no longer be seen and *Q*-scores become very low.

At 3.1 Å resolution, both Mg atoms still have moderately high *Q*-scores, and they are inside the map contour at lower threshold. It appears that even at such lower resolutions, ions can significantly influence cryo-EM map values. Thus even at these resolutions, solvent atoms may perhaps be considered in the model, particularly if known structures of the same complex at higher resolutions also contain such atoms. Consequently, this may improve the accuracy of side chain positions and rotameric configurations during refinement.

Discussion

Q-scores measure the resolvability of individual atoms in a cryo-EM map, using an atomic model fitted to or built into the map. It should

be noted that nothing is assumed about the model itself, for example whether it has good stereochemistry; this could be deduced with other scores such as the Molprobity score[31]. *Q*-scores averaged over entire models correlate very closely to the reported resolution of the maps in which they are calculated. The score can also be useful to analyze the map and its resolvability in different regions, and also test whether the model may need further refinement in some areas as indicated by low *Q*-scores. Here, *Q*-scores were also applied to various maps at different resolutions to show quantifiable trends across different side chains in proteins, bases in nucleic acids, and also to assess the resolvability of solvent atoms and ions. *Q*-scores should continue to be a useful metric in the analysis of cryo-EM maps and models.

Online content

Any methods, additional references, Nature Research reporting summaries, source data, extended data, supplementary information, acknowledgements, peer review information; details of author contributions and competing interests; and statements of data and code availability are available at https://doi.org/10.1038/s41592-020-0731-1.

Received: 5 August 2019; Accepted: 31 December 2019;
Published online: 10 February 2020

References

1. Anonymous. Challenges for cryo-EM. *Nat. Methods* **15**, 985–985 (2018).
2. Henderson, R. et al. Outcome of the first electron microscopy validation task force meeting. *Struct. Lond. Engl. 1993* **20**, 205–214 (2012).
3. Kucukelbir, A., Sigworth, F. J. & Tagare, H. D. Quantifying the local resolution of cryo-EM density maps. *Nat. Methods* **11**, 63–65 (2014).
4. Heymann, J. B. Guidelines for using Bsoft for high resolution reconstruction and validation of biomolecular structures from electron micrographs. *Protein Sci. Publ. Protein Soc.* **27**, 159–171 (2018).
5. Anonymous. Local resolution of cryo-EM maps with MonoRes. *Nat. Methods* **15**, 246 (2018).
6. Pintilie, G. & Chiu, W. Comparison of Segger and other methods for segmentation and rigid-body docking of molecular components in cryo-EM density maps. *Biopolymers* **97**, 742–760 (2012).
7. Terwilliger, T. C., Adams, P. D., Afonine, P. V. & Sobolev, O. V. A fully automatic method yielding initial models from high-resolution cryo-electron microscopy maps. *Nat. Methods* **15**, 905 (2018).
8. Joseph, A. P., Lagerstedt, I., Patwardhan, A., Topf, M. & Winn, M. Improved metrics for comparing structures of macromolecular assemblies determined by 3D electron-microscopy. *J. Struct. Biol.* **199**, 12–26 (2017).
9. Afonine, P. V. et al. Real-space refinement in PHENIX for cryo-EM and crystallography. *Acta Crystallogr. D.* **74**, 531–544 (2018).
10. Trabuco, L. G. et al. Applications of the molecular dynamics flexible fitting method. *J. Struct. Biol.* **173**, 420–427 (2011).
11. Joseph, A. P. et al. Refinement of atomic models in high resolution EM reconstructions using Flex-EM and local assessment. *Methods* **100**, 42–49 (2016).
12. Pintilie, G., Chen, D.-H., Haase-Pettingell, C. A., King, J. A. & Chiu, W. Resolution and probabilistic models of components in cryoEM maps of mature P22 bacteriophage. *Biophys. J.* **110**, 827–839 (2016).
13. DiMaio, F., Zhang, J., Chiu, W. & Baker, D. Cryo-EM model validation using independent map reconstructions. *Protein Sci.* **22**, 865–868 (2013).
14. Trabuco, L. G., Villa, E., Schreiner, E., Harrison, C. B. & Schulten, K. Molecular dynamics flexible fitting: a practical guide to combine cryo-electron microscopy and X-ray crystallography. *Methods* **49**, 174–180 (2009).
15. DiMaio, F., Tyka, M. D., Baker, M. L., Chiu, W. & Baker, D. Refinement of protein structures into low-resolution density maps using rosetta. *J. Mol. Biol.* **392**, 181–190 (2009).
16. Barad, B. A. et al. EMRinger: side chain-directed model and map validation for 3D cryo-electron microscopy. *Nat. Methods* **12**, 943–946 (2015).
17. Pintilie, G. & Chiu, W. Assessment of structural features in Cryo-EM density maps using SSE and side chain Z-scores. *J. Struct. Biol.* **204**, 564–571 (2018).
18. Zivanov, J. et al. New tools for automated high-resolution cryo-EM structure determination in RELION-3. *eLife* **7**, e42166 (2018).
19. Dunitz, J. D., Schomaker, V. & Trueblood, K. N. Interpretation of atomic displacement parameters from diffraction studies of crystals. *J. Phys. Chem.* **92**, 856–867 (1988).
20. Trueblood, K. N. et al. Atomic dispacement parameter nomenclature. Report of a subcommittee on atomic displacement parameter nomenclature. *Acta Crystallogr. A.* **52**, 770–781 (1996).
21. Carugo, O. How large B-factors can be in protein crystal structures. BMC Bioinformatics 19, https://doi.org/10.1186/s12859-018-2083-8 (2018).
22. Hyrc, C. F. et al. Accurate model annotation of a near-atomic resolution cryo-EM map. *Proc. Natl Acad. Sci. USA* **114**, 3103–3108 (2017).
23. Herzik, M. A., Fraser, J. S. & Lander, G. C. A multi-model approach to assessing local and global cryo-EM map quality. *Struct. Lond. Engl. 1993* **27**, 344–358.e3 (2019).
24. Singharoy, A. et al. Molecular dynamics-based refinement and validation for sub-5 Å cryo-electron microscopy maps. *eLife* **5**, e16105 (2016).
25. Meyder, A., Nittinger, E., Lange, G., Klein, R. & Rarey, M. Estimating electron density support for individual atoms and molecular fragments in X-ray structures. *J. Chem. Inf. Model.* **57**, 2437–2447 (2017).
26. Wahab, M. A. *Essentials of Crystallography* (Alpha Science International, 2009).
27. Graef, M. D. Introduction to Conventional Transmission Electron Microscopy (Cambridge Univ. Press, 2003).
28. Holton, J. M. A beginner's guide to radiation damage. *J. Synchrotron Radiat.* **16**, 133–142 (2009).
29. Darby, J. F. et al. Water networks can determine the affinity of ligand binding to proteins. *J. Am. Chem. Soc.* **141**, 15818–15826 (2019).
30. Emsley, P. & Cowtan, K. Coot: model-building tools for molecular graphics. *Acta Crystallogr. D.* **60**, 2126–2132 (2004).
31. Chen, V. B. et al. MolProbity: all-atom structure validation for macromolecular crystallography. *Acta Crystallogr. D.* **66**, 12–21 (2010).

Publisher's note Springer Nature remains neutral with regard to jurisdictional claims in published maps and institutional affiliations.

© The Author(s), under exclusive licence to Springer Nature America, Inc. 2020

Methods

Cryo-EM. Human apoferritin samples were provided by F. Sun and X.J. Huang (Institute of Biophysics, CAS). Images of the sample were collected in Titan Krios electron microscope (Thermo Fisher) at 300 keV, equipped with BioQuantum energy filter and K2 director detector (Gatan). A total of 1,100 images were recorded in movie mode. Motion correction was performed with MotionCor2 (ref. [32]) (v.1.1.0). Particles were picked using the EMAN2 neural network particle picker[33] (EMAN2 v.2.22). Three-dimensional reconstruction was performed using Relion[18] (v.3.0). Map resolution was estimated from two independently reconstructed maps. Three maps of apoferritin were reconstructed using different number of particles: 1.75 Å using 70,648 particles, 2.3 Å using 9,600 particles and 3.1 Å using 495 particles. All three maps were reconstruction with octahedral symmetry.

Models. The X-ray model PDB 3ajo of human apoferritin was rigidly fitted to each new apoferritin cryo-EM map using the Segger[6] plugin in UCSF Chimera[34] (v.2.3), and refined using Phenix real-space refinement[9] (v.1.14 build 3260). *Q*-score calculations were performed with the MapQ plugin[35] to UCSF Chimera (v.1.2).

Statistical analysis. The Pearson correlation (*r*) values for *Q*-scores versus reported resolution (plotted in Fig. 5) were calculated using Python and the scipy.stats. linregress function. The reported r_value was squared to obtain r^2 in each case. In these figures, the number of data points is the number of entries in the respective table (Supplementary Table 1 for Fig. 5a and Supplementary Table 2 for Fig. 5b). For all figures, since the methods used are deterministic, the measurements were only performed once to obtain the displayed values.

Reproduction instructions. To reproduce *Q*-scores shown in the various images, the maps and models indicated can be downloaded from EMDB and PDB. For the apoferritin examples, the models may first have to be rigidly fitted to the density (for example, using Chimera/Segger/Fit to Segments), and then refined using Phenix.real_space_refinement. Then, *Q*-scores can be calculated using the MapQ plugin (https://github.com/gregdp/mapq). For more details, see tutorials/MapQ_Tutorial.pdf at the link.

The statistical analysis (*Q*-scores versus map resolution), can be reproduced using the same approach, downloading the maps and models indicated in Supplementary Tables 1 and 2. *Q*-scores can also be calculated for maps and model from the command line, making it easier to run a large batch of maps and models (see documentation/QScores_CommandLine.docx at the github link above).

Reporting Summary. Further information on research design is available in the Nature Research Reporting Summary linked to this article.

Data availability

The cryo-EM maps of apoferritin have been deposited in the EMDB with accession codes 20026 (1.75 Å), 20027 (2.3 Å) and 20028 (3.1 Å). The figures show these maps and also other maps and models available in the EMDB and PDB (accession codes specified in the figure captions, see also Supplementary Tables 1 and 2). All data including calculations based on these maps that support the findings of this study are available from the corresponding author upon request.

Code availability

Q-scores are implemented in the MapQ plugin to UCSF Chimera and available on GitHub and Zenodo[35]. A tutorial is also available at the link under the 'tutorials' folder. Pseudo code is provided under the 'docs' folder.

References

32. Zheng, S. Q. et al. MotionCor2: anisotropic correction of beam-induced motion for improved cryo-electron microscopy. *Nat. Methods* **14**, 331–332 (2017).
33. Bell, J. M., Chen, M., Durmaz, T., Fluty, A. C. & Ludtke, S. J. New software tools in EMAN2 inspired by EMDatabank map challenge. *J. Struct. Biol.* **204**, 283–290 (2018).
34. Pettersen, E. F. et al. UCSF Chimera—a visualization system for exploratory research and analysis. *J. Comput. Chem.* **25**, 1605–1612 (2004).
35. Pintilie, G. MapQ (GitHub, 2019); https://github.com/gregdp/mapq

Acknowledgements

This research has been supported by National Institutes of Health grants (nos. R01GM079429, P41GM103832 and S10OD021600) to W.C. Molecular graphics and analyses were performed with the UCSF Chimera package. Chimera is developed by the Resource for Biocomputing, Visualization and Informatics at the University of California, San Francisco (supported by grant no. NIGMS P41GM103311). We thank F. Sun and X.J. Huang (Institute of Biophysics, CAS) for the human apoferritin samples. We also thank C. Lawson for discussions related to B-factors and ADPs.

Author contributions

G.P. and W.C. conceived *Q*-scores. G.P. implemented the software and performed testing. K.Z. collected the images and reconstructed the maps (EMDB 20026, 20027 and 20028). Z.S. and S.L. provided additional data (not shown) for testing the *Q*-score. M.F.S. and W.C. contributed the discussion during the development. G.P. wrote the manuscript with inputs from other authors.

Competing interests

The authors declare no competing interests.

Additional information

Supplementary information is available for this paper at https://doi.org/10.1038/s41592-020-0731-1.

Correspondence and requests for materials should be addressed to G.P. or W.C.

Reprints and permissions information is available at www.nature.com/reprints.

nature research

Corresponding author(s): Grigore Pintilie, Wah Chiu

Last updated by author(s): Dec 3, 2019

Reporting Summary

Nature Research wishes to improve the reproducibility of the work that we publish. This form provides structure for consistency and transparency in reporting. For further information on Nature Research policies, see Authors & Referees and the Editorial Policy Checklist.

Statistics

For all statistical analyses, confirm that the following items are present in the figure legend, table legend, main text, or Methods section.

n/a	Confirmed	
☐	☒	The exact sample size (*n*) for each experimental group/condition, given as a discrete number and unit of measurement
☐	☒	A statement on whether measurements were taken from distinct samples or whether the same sample was measured repeatedly
☐	☒	The statistical test(s) used AND whether they are one- or two-sided *Only common tests should be described solely by name; describe more complex techniques in the Methods section.*
☐	☒	A description of all covariates tested
☐	☒	A description of any assumptions or corrections, such as tests of normality and adjustment for multiple comparisons
☐	☒	A full description of the statistical parameters including central tendency (e.g. means) or other basic estimates (e.g. regression coefficient) AND variation (e.g. standard deviation) or associated estimates of uncertainty (e.g. confidence intervals)
☐	☒	For null hypothesis testing, the test statistic (e.g. *F*, *t*, *r*) with confidence intervals, effect sizes, degrees of freedom and *P* value noted *Give P values as exact values whenever suitable.*
☐	☒	For Bayesian analysis, information on the choice of priors and Markov chain Monte Carlo settings
☐	☒	For hierarchical and complex designs, identification of the appropriate level for tests and full reporting of outcomes
☐	☒	Estimates of effect sizes (e.g. Cohen's *d*, Pearson's *r*), indicating how they were calculated

Our web collection on statistics for biologists contains articles on many of the points above.

Software and code

Policy information about availability of computer code

Data collection	FEI EPU (v2.1)
Data analysis	MotionCor2 (v1.1.0), EMAN2 (v2.22), Relion (v3.0), UCSF Chimera (v1.13 build 41780), Segger (v2.3), MapQ Plugin (v1.2), Phenix (v1.14 build 3260)

For manuscripts utilizing custom algorithms or software that are central to the research but not yet described in published literature, software must be made available to editors/reviewers. We strongly encourage code deposition in a community repository (e.g. GitHub). See the Nature Research guidelines for submitting code & software for further information.

Data

Policy information about availability of data

All manuscripts must include a data availability statement. This statement should provide the following information, where applicable:

- Accession codes, unique identifiers, or web links for publicly available datasets
- A list of figures that have associated raw data
- A description of any restrictions on data availability

The new cryoEM maps of Apoferritin have been deposited in the EMDB with accession codes 20026 (1.75Å), 20027 (2.3Å), and 20028 (3.1Å). The figures show these maps and also other maps and models available in the EMDB and PDB (accession codes specified in Figures text, also Tables 1 and 2). There are no restrictions on data availability as long as the EMDB and PDB can be accessed.

Field-specific reporting

Please select the one below that is the best fit for your research. If you are not sure, read the appropriate sections before making your selection.

☒ Life sciences ☐ Behavioural & social sciences ☐ Ecological, evolutionary & environmental sciences

For a reference copy of the document with all sections, see nature.com/documents/nr-reporting-summary-flat.pdf

Life sciences study design

All studies must disclose on these points even when the disclosure is negative.

Sample size	1100 images (micrographs) of the human apoferritin protein sample were collected using a Titan Krios microscope. The sample was obtained from F. Sun and X.J. Huang (Institute of Biophysics, CAS).
Data exclusions	From the 1100 images, particles were picked using the EMAN2 neural network particle picker. After motion correction with MotionCorr2 and 3D reconstruction with Relion, 70,648 particles were finally used to reconstruct the final 1.75Å cryoEM map. Some particles initially picked may have been discarded during this process if they are found to not be consistent with the map refined at each step.
Replication	The 1100 images were split into two halves, and the entire process was repeated to obtain 2 independent maps of the same specimen. The two maps were very similar to the final map. An FSC plot between these two independent maps estimates a resolution of 1.75Å for the final map.
Randomization	Particles were further excluded randomly to arrive at lower resolution maps (for comparison purposes). A total of 9600 particles were randomly picked and used to obtain a 2.3Å map, and 495 particles were randomly picked to obtain a 3.1Å map.
Blinding	Blinding was not used in this work.

Reporting for specific materials, systems and methods

We require information from authors about some types of materials, experimental systems and methods used in many studies. Here, indicate whether each material, system or method listed is relevant to your study. If you are not sure if a list item applies to your research, read the appropriate section before selecting a response.

Materials & experimental systems

n/a	Involved in the study
☒	☐ Antibodies
☒	☐ Eukaryotic cell lines
☒	☐ Palaeontology
☒	☐ Animals and other organisms
☒	☐ Human research participants
☒	☐ Clinical data

Methods

n/a	Involved in the study
☒	☐ ChIP-seq
☒	☐ Flow cytometry
☒	☐ MRI-based neuroimaging